

Stiffening of Individual Fibrin Fibers Equitably Distributes Strain and Strengthens Networks

Nathan E. Hudson,[†] John R. Houser,[†] E. Timothy O'Brien III,[†] Russell M. Taylor II,^{†§¶} Richard Superfine,[†] Susan T. Lord,[‡] and Michael R. Falvo^{†*}

[†]Department of Physics and Astronomy, [‡]Department of Pathology and Laboratory Medicine, [§]Department of Computer Science, and [¶]Curriculum in Applied Sciences and Engineering, University of North Carolina at Chapel Hill, Chapel Hill, North Carolina

ABSTRACT As the structural backbone of blood clots, fibrin networks carry out the mechanical task of stemming blood flow at sites of vascular injury. These networks exhibit a rich set of remarkable mechanical properties, but a detailed picture relating the microscopic mechanics of the individual fibers to the overall network properties has not been fully developed. In particular, how the high strain and failure characteristics of single fibers affect the overall strength of the network is not known. Using a combined fluorescence/atomic force microscope nanomanipulation system, we stretched 2-D fibrin networks to the point of failure, while recording the strain of individual fibers. Our results were compared to a pair of model networks: one composed of linearly responding elements and a second of nonlinear, strain-stiffening elements. We find that strain-stiffening of the individual fibers is necessary to explain the pattern of strain propagation throughout the network that we observe in our experiments. Fiber strain-stiffening acts to distribute strain more equitably within the network, reduce strain maxima, and increase network strength. Along with its physiological implications, a detailed understanding of this strengthening mechanism may lead to new design strategies for engineered polymeric materials.

INTRODUCTION

Fibrin fiber networks form the major structural framework of blood clots, and their mechanical properties determine clot strength and stability (1). The failure of these networks can lead to embolism, the process in which a portion of a clot breaks away and is carried downstream by the flowing blood. This can result in a variety of adverse consequences including stroke and pulmonary damage; thus, the details of how the clot fails and the associated role of the mechanics of the fibrin network are of critical biomedical relevance.

Fibrin networks belong to a class of biological materials that display a remarkable and diverse set of mechanical properties including high extensibility, nonlinear elasticity (strain-stiffening) and negative normal stress (2–12). Although these behaviors have been well characterized in macroscopic studies, an understanding of their molecular and fiber-level origins has only recently begun to develop (8,10,13,14). To construct a complete multiscale picture of network behavior, a thorough characterization of microscopic properties must be accompanied by an understanding of how they conspire to produce the emergent bulk response under stress: How do the single fiber properties translate into the bulk properties of the network?

Materials strength—the maximum stress a material can withstand before failure—is particularly dependent on microscopic mechanical and geometrical details. Failure occurs at points of concentrated stress or points of mechanical weakness; it is determined by extreme values in the

range of microscopic properties rather than in their average values. This is in contrast to properties, such as elastic moduli, which are amenable to a mean field analysis. A thorough understanding of how a fibrin network fails—a question of profound biomedical as well as materials interest—requires a detailed look at how individual fibrin fibers stretch, how they distribute strain, and ultimately how they fail. Modeling studies focusing on the mechanics of biopolymer networks identify two phenomena responsible for a network's response to stress: stiffening behavior of the constituent fibers and geometrical rearrangement of the fibers (10,14–16). The balance struck between these two mechanisms depends in large part on the flexibility of the fiber segments comprising the network. Models of semiflexible fibers—fiber elements with persistence lengths comparable to their contour lengths—show that stiffening of a network can arise from the entropic stiffening of the constituent fibers comprising the network (14). On the other hand, models of stiff fibers show that stiffening develops from a geometrical reorientation and transition from bending at small strains to enthalpic stretching at larger strains (16). Although these models have been successful at describing network behavior at low strains (13,14), the question of how the stiffening and re-arrangement of individual fibers affects stress and strain distribution and ultimately the overall network strength at high fiber strains, has received less attention.

Recent experimental work has begun to bridge the gap between bulk macroscopic properties and their origins at the individual fiber level. Advances in micro- and nanoscale interrogative techniques have enabled mechanical studies of fibrin at the single fiber (17–20) and molecular scale (21–23).

Submitted September 9, 2009, and accepted for publication December 8, 2009.

*Correspondence: falvo@physics.unc.edu

Editor: Denis Wirtz.

© 2010 by the Biophysical Society
0006-3495/10/04/1632/9 \$2.00

doi: 10.1016/j.bpj.2009.12.4312

These studies showed that individual fibrin fibers possess remarkable elastic properties; they are capable of reversibly stretching as much as three times their original length, and can more than quadruple their length before breaking (18–20). We also report direct measurements that show fibrin fibers themselves exhibit nonlinear elasticity. The molecular origins of these properties are still an open question, but recent studies have implicated several different regions of the fibrin molecule as possible sources for fibrin's extensibility including the coiled-coil region (10,21,22), the globular γ domain (23), and the α C connector region (20). Further investigation is needed, but it is clear that the fibrin fibers themselves exhibit elastomeric behavior: low elastic modulus in stretching (MPa) and very high extensibility (>300%).

Within fibrin networks, microscopic measurements of filament reorientation and alignment under stress have been made both at low strains in a shear cell (8,13) and at high tensile strains (10). At high network strain, the fibers have aligned in the direction of the stress, and fiber stretching is the dominant deformation mechanism. Consequently, the elastomeric properties of the individual fiber dramatically affect network deformation in this regime, and play a direct role in determining network strength: failure originates ultimately at a single fiber (or branch point). Thus, network strength is determined by the maximum strain individual fibers can withstand. Determining how strain is shared among the constituent fiber segments in a network under imposed stress is therefore crucial to understanding failure modes of networks and their strength. We describe here that the strain-stiffening of the individual fibrin fibers produces a dramatic shift in strain distribution and effectively strengthens fibrin networks.

MATERIALS AND METHODS

Fibrinogen

All experiments used recombinant human fibrinogen produced in Chinese hamster ovary cells (24,25). Fibrin clots formed with recombinant human fibrinogen are indistinguishable from clots formed with plasma fibrinogen. Recombinant fibrinogen was used in this study because it is free from other blood coagulation factors, in particular, FXIII (25). Fibrinogen purity and homogeneity was assessed by SDS polyacrylamide gel electrophoresis and immunoblot analyses. Fibrinogen function was assessed through thrombin-catalyzed polymerization monitored by turbidity, and FXIIIa-catalyzed cross-linking monitored by SDS polyacrylamide gel electrophoresis (26).

Structured surfaces and sample prep

Fibrin fibers and networks were assembled *in situ* onto Norland Optical cured structured surfaces as described previously (18). Briefly, a polydimethylsiloxane (PDMS) (Sylgard 184; Dow Corning Corp., Midland, MI) stamp with 20- μ m wide and 10- μ m deep channels was placed on a small drop of Norland Optical #81 (an ultraviolet-light-curable optical adhesive) (Norland Products, Inc., Cranbury, NJ) in the middle of a 24 \times 50 mm 1.5 cover glass (Corning, Lowell, MA). The adhesive was polymerized with long wavelength ultraviolet light for 2 min, and the stamp was peeled off, leaving a cured structured surface (SS).

Before use, the SS was cleaned for an additional 2 min in an ultraviolet cleaner, and a ring of silicon grease was applied with a cotton swab to confine fibrin assembly to the SS. Fibrinogen, stored at 0.6 mg/mL, thrombin (human α -thrombin; Enzyme Research Labs, Indianapolis, IN), stored at 222 U/mL, and Factor XIII (human plasma FXIII; Enzyme Research Labs), stored at 68 μ g/mL at -80° C were thawed rapidly and placed on ice. Fibrinogen and FXIII were diluted to 0.04 mg/mL and 0.1 μ g/mL, respectively, in 20 mM HEPES, 150 mM NaCl, pH 7.4 (HBS), and 50% the final volume needed to cover the SS (\sim 8–10 μ L) was pipetted onto the surface. Thrombin was diluted just before use to 2 U/mL in HBS with 10 mM CaCl₂, and an equal volume was added to each SS and mixed by gently pipetting up and down several times. Final concentrations of reagents were: 0.02 mg/mL fibrinogen, 1.0 U/mL thrombin, 0.05 μ g/mL Factor XIII in HBS, and 5 mM calcium.

Coverslips with fibrin reactions were placed in petri dishes with a small square of wet paper towel to prevent drying, and incubated at 37°C for 2 h. Thrombin catalyzed the conversion of FXIII to FXIIIa and fibrinogen to fibrin forming crosslinked fibers as evidenced by gel electrophoresis. The reaction solution was removed and the samples washed twice with HBS. Twenty-four nanometers of volume-labeled red fluorescent carboxyl-coated microspheres (stock comes at 2% solid in water; Invitrogen, Carlsbad, CA) were diluted 1/10,000 in HBS and added to each SS; samples were incubated for 5 min, washed with HBS, and used for experiments.

Samples were prepared with and without FXIII that is converted into FXIIIa in the presence of thrombin and calcium. Samples without FXIII were prepared in the same manner, without the addition of FXIII and incubating for only 15 min.

Optical microscopy

For observation and manipulation of fibers, the coverslips were placed face up on an inverted Nikon Diaphot 200 microscope with epifluorescence illumination (Southern Micro Instruments, Atlanta, GA), and imaged using a rhodamine HQ filter set (Chroma Technology, Rockingham, VT) and a 1.3 or 1.4 NA 100 \times oil objective. Images were recorded using a high speed Cooke PCO 1600 camera with C-link and recorded with CamWare (Cooke Corporation, Romulus, MI). All single fiber and network data were acquired as described previously (18,19).

Atomic force microscope

The atomic force microscope (AFM; Explorer, Veeco Instruments, Woodbury, NY) rests on the manipulation stage of the optical epifluorescence microscope enabling simultaneous AFM manipulation and optical data acquisition. Both OMCL-AC240TS-W2 (Olympus, Asylum Research, Santa Barbara, CA, Micro Cantilever) and RC150VB Biolever (Olympus, Asylum Research) AFM cantilevers (SiN) were used for manipulation. A detailed description of our setup and measurement can be found in prior publications (18,19). Briefly, force data were determined through calibration of the lateral deflection signal. The angular optical sensitivity of the twisting mode is the same as for the bending mode given we have a geometrically symmetric quadrant photodiode and similar gain settings for each quadrant. The twisting mode optical sensitivity in deflection units is then determined using the specific geometry (length, tip length) of the cantilever. The lateral cantilever spring constant was calculated from cantilever/geometry and SiN materials constants. The AFM tip was controlled using the Nanomanipulator software (3rdTech, Durham, NC). The tip was set down inside the network and moved in one direction at 1 μ m/s in 75-nm increment steps to stretch the network. To facilitate the tracking of individual fibers using Video Spot Tracker software (Computer Integrated Systems for Microscopy and Manipulation at UNC-Chapel Hill (<http://www.cisimm.org/>)), networks containing 10–30 distinct fibers all around 1–10 μ m in length and in the same plane of focus were selected for manipulation. Networks were stretched until failure of the pulled fiber; but when analyzing the data the network was considered to fail at the first rupture of any junction or fiber, not just the pulled fiber. Fig. 1 depicts a diagram of the setup. Fiber diameters were determined

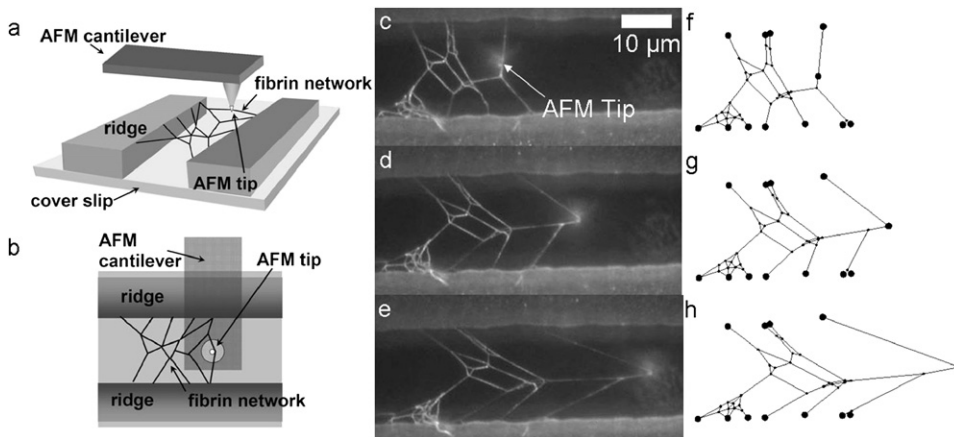


FIGURE 1 Experimental setup: (a and b) Side and bottom views depicting the AFM and a fibrin network suspended between ridges. (c–e) Three time point snapshots of a network undergoing deformation due to AFM manipulation. (f–h) Model network deformations at equivalent points to c–e.

with AFM topographical imaging. Fibers extending onto the ridge surface were located with fluorescence imaging. The AFM tip was engaged in proximity to the fiber and local imaging was carried out.

Network strain measurements

Strain measurements on individual fibers within each network were calculated using video data recorded during the network manipulation (Fig. 2). Strain was calculated for each fiber, measuring the change in the distances between junctions. In both FXIIIa ligated and unligated networks, fibers junctions were not observed sliding or slipping along the fibers during the pull; instead junctions appeared fixed with respect to the fiber. Data were only collected from samples for which fiber attachments to the ridge boundaries were fixed throughout the stretching. The fibers are adhered to the ridge through nonspecific adhesion. Given the relatively low forces involved in the pulling experiments versus the relatively high adhesive forces of the fibrin to the ridge, it is not surprising that they typically maintain fixed boundary attachments. Fibers pulled by the tip were assumed to converge to a point, for comparison with simulations. Manual distance measurements using the line segment measurement tool in the ImageJ (<http://rsbweb.nih.gov/ij/>) software package supplemented the automated software, especially for junctions that Video Spot Tracker had difficulty tracking. Usually four to eight fibers per network were tracked; the fibers tracked were selected based

on original fiber length, focus, position relative to glue stamped surfaces and point of pull. We did not track fibers attached to the surfaces. Fiber strain was then plotted as a function of AFM tip movement. The derivative of the strain versus AFM step plots, dubbed the strain fraction, was calculated by taking the average slope between 10 points on strain versus AFM step data (Fig. 2). The slope was then smoothed using the MATLAB R2007b (The MathWorks, Natick, MA) *rhoess* function.

Webslinger

Networks were simulated using Webslinger (<http://www.cisimm.org/>), a quasistatic mass-spring simulation that uses Euler integration with small timesteps and damping to solve the system of partial differential equations governing a network of springs. After each step, the system is allowed to relax to equilibrium, and that solution is used for the initial conditions of the next step.

Arbitrary nonlinear spring behavior was specified by providing force-strain curves and rest lengths for each spring. For each experimental network geometry, a mesh model of the same geometry (node location accuracy within 150–200 nm) was created by hand from the video file image (Fig. 1). Wall boundary nodes were simulated as immovable, but freely rotating pivot positions. The mesh node corresponding to location of the AFM tip was moved along the same trajectory taken by the tip in the

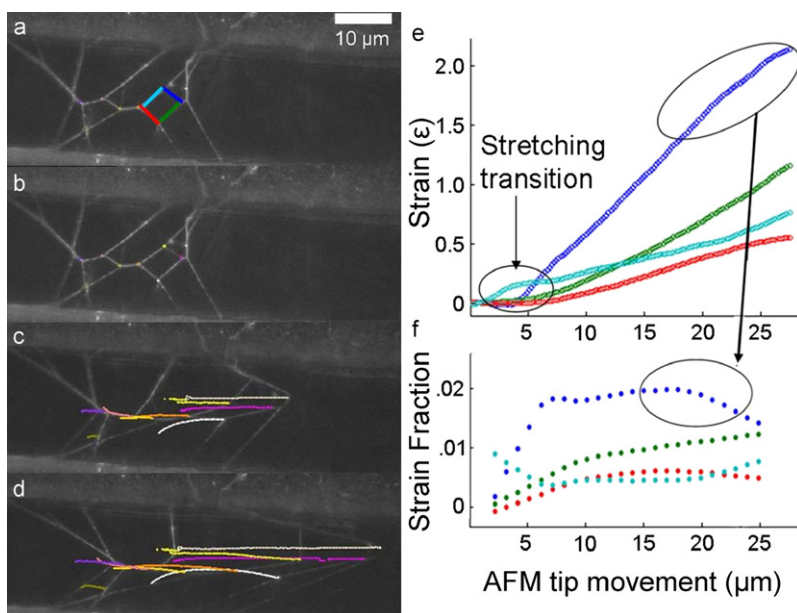


FIGURE 2 Network strain measurements. (a–d) Images from a video of network deformation. (a) The original network geometry highlighting four fibers whose strain will be tracked throughout the network deformation (plotted in frames e–f). (b–d) Fiber nodes in the network were selectively tracked, and fiber strains were calculated using the distances between the nodes. The lines in c and d show tracking data, tracing the motion of network junctions throughout the deformation. (e) A plot of individual fiber strain versus AFM tip movement. Each trace represents the strain versus AFM tip movement for one fiber corresponding to frame a. (f) The strain fraction (derivative of strain with respect to tip movement, or slope, of plot in e). The circled data in the lower left of the plot in e indicates the stretching transition where fibers are reorienting and beginning to stretch. The other circles on the right side highlight a concave downward trend in the strain plot e) and the corresponding decrease in the strain fraction f) for the most strained fiber (top trace). Note also that the strain fraction of the several lesser strained traces trends upward in the strain fraction plot (f) at high AFM tip movement. These trends indicate that as the most strained fiber stiffens, it transfers strain share to the less strained, softer fibers.

experiment. (Fig. 1) Patterns of fiber strain distribution within the simulated networks were then compared to those seen in the fibrin network experiments. Two force-strain curves were used for the comparison with fibrin data, a linear model, and a worm-like chain force model.

RESULTS

Using a combined fluorescence microscope and AFM, we stretched fibrin networks to failure and measured the tensile strain of individual constituent fibers. Focusing on small, (5–30 fibers) 2-D fibrin networks suspended between microprinted channels, we obtained a complete view of network geometry during deformation (Fig. 1). For each network, the AFM tip was placed next to a fiber located at the periphery of the network, and that fiber was pulled in a direction parallel to the channel axis (Fig. 2, *a–d*). Usually networks were pulled to the point of failure, but in some instances, networks slipped off the tip before failing and elastically recovered their original structure. Additionally, several experiments were carried out where the network was stretched out 20 μm and then stepped back to its original position with no observable damage. These results indicate that network deformations were reversible for fiber strains ≤ 1.0 .

Five to ten fibers in close proximity to the point of pull were selected for strain measurements. The tensile strain of each tracked fiber in the network was plotted as a function of AFM tip movement (Fig. 2 *e* and Fig. 3). At low strains, there was a noticeable transition regime in which all fibers began stretching more per incremental AFM tip movement. This is a geometrical effect; the fibers reorient, aligning in the direction of the applied force before entering a tensile stretching mode. When the most-strained fibers in the network reached strains >1.0 , there was a noticeable decrease in strain per incremental AFM tip movement.

That is, the change in strain with respect to tip movement decreased for the most-strained fibers (Fig. 2 *f*, *top trace*). This derivative or strain fraction, reflects the share the overall network deformation taken on by each fiber per incremental AFM step. Accompanying the decrease in strain fraction of the most strained fibers, the strain fraction of lesser strained fibers commonly increased (Fig. 2 *f*, *middle traces*). The two potential sources of this behavior are network geometry and individual fiber properties. In the former, the strain share (the distribution or sharing of the overall network deformation among the individual fibers) shifts as the network architecture reorients and gradually aligns in the direction of the applied force. Alternatively, the nonlinear elasticity of the individual fibers redistributes the strain share as some fibers stiffen relative to the others. These two phenomena are not mutually exclusive and could both be contributing factors.

To assess the potential contributions of fiber nonlinear elasticity to network deformation, we measured the force elongation behavior of individual fibrin fibers using a similar experimental approach (18,19). Individual fibers were suspended between microprinted channels and force data were obtained from calibrated lateral deflection of the AFM cantilever. The data showed a clear transition from low stiffness and linear elasticity at low strain to much higher stiffness at strains at or above 1.0 (Fig. 4). This characteristic strain stiffening force versus elongation relation was used to quantitatively inform modeling of our network data.

Network modeling

To separate the effect of network geometry from the effect of the nonlinear stiffness of the constituent fibers, experimental results were compared with quasistatic mass-spring simulations. Each experimental network was modeled by a simulated network of equivalent geometry. AFM stretching was

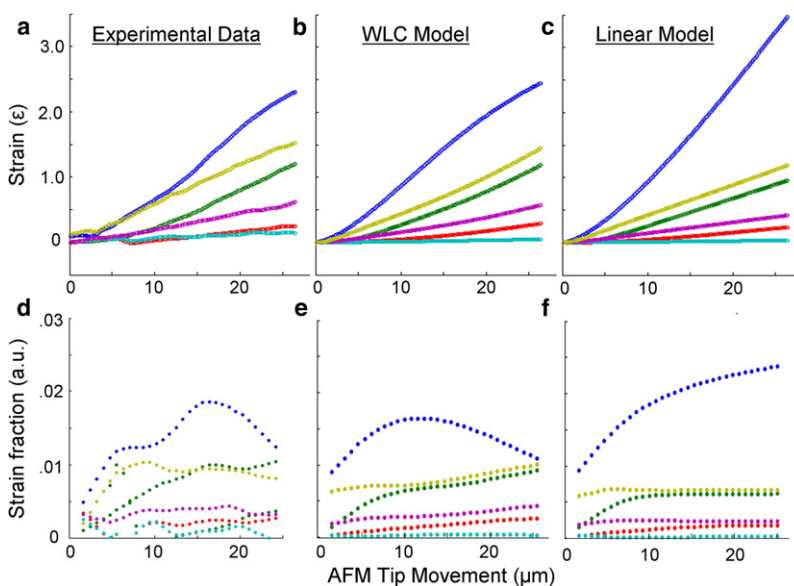


FIGURE 3 Experiment versus simulations. (*a–c*) Fiber strain traces for a particular experimental network and for simulations of equivalent WLC and linear model networks. (*d–f*) Plots of the strain fraction corresponding to *a–c*. The experimental strain and strain fraction data show a much closer correspondence to the WLC model than to the linear network particularly for the most strained fibers at high AFM tip movement. Two predominant features contrast the experiment and WLC model data from the linear model. First, the linear model shows much higher maximum strain (*top trace. c*) than either experiment (*a*) or WLC model (*b*). Second, within the strain fraction plots, the most strained fiber (*top trace. c*) shows a clear decrease above tip movement of 15 μm for both the experiment and WLC model, whereas the linear model shows no such decrease. The strain fractions of the fibers in the linear model approach constant and highly dispersed values indicating each fiber takes on constant and inequitable strain share. The strain fraction of the experimental and WLC model fibers converge into a much narrower range at high AFM tip movement indicating that strain share is transferring from the most strained to the lesser strained fibers, more equitably distributing strain throughout the network.

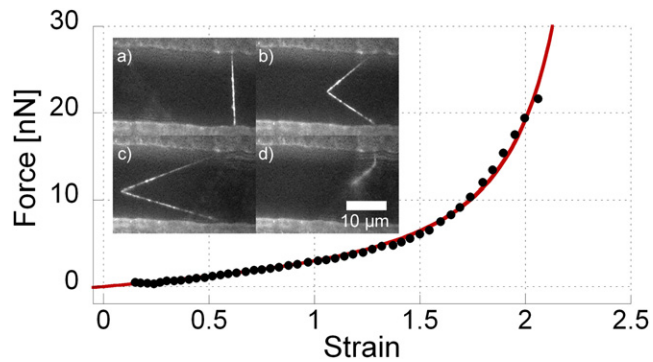


FIGURE 4 Single fibrin fiber force curve: Inset (a–d) depicts a single suspended fiber stretched to breaking (d) by an AFM tip. (Plot) The black points depict single fibrin fiber force-strain data determined by calibrated lateral AFM force measurement. The geometrical aspects of the measurement were taken into account to convert raw AFM force data to fiber tensile force. The strain of the fiber was determined from the calibrated video data. The line through the data depicts the WLC fit using two fitting parameters: the persistence and contour lengths.

replicated by incrementally moving the point (a mass node in the model) corresponding to the AFM/fiber contact in the experiment. AFM imaging of fibers extending onto the structured surface ridges indicated an average diameter of 80 ± 20 nm (we found no statistical difference between ligated and unligated clots). However, due to the limited feasibility of accurately determining fiber diameters within the network before the pull (fibers suspended between the ridges could not be imaged with the AFM and the SEM preparation would alter network mechanical properties), we have assumed that all fibers have equal diameter. Although the equal diameter assumption is not ideal, it is supported by fluorescent confocal microscopy and SEM studies of *in vitro* clots that show a relatively narrow variation in fiber diameter (15–30% (6,27)). As a consequence of this assumption, each fiber segment has a common force versus strain relation. Two force extension models were implemented: a linear springs model and a nonlinear strain stiffening model.

Within the linear springs model, each fiber segment is a linear spring with a spring constant inversely proportional to its original length (as is the case for an ideal spring), $k = \kappa/L_0$, where κ plays the role of spring constant in a force versus strain relationship. This provides each fiber segment with the same force versus strain relation, regardless of its length ($F = \kappa \varepsilon$).

We modeled the nonlinear single fiber force versus extension behavior (Fig. 4), using an ideal chain model known as the worm-like chain (WLC). This model has successfully described the force-extension behavior of intrinsically unstructured polypeptides as well as force-unfolded proteins (28–32). Our purpose in using the WLC is to apply a force versus extension model that reflects the single fiber stretching data. Marko and Siggia (33) approximated a force versus extension relationship for the WLC model in the context of DNA stretching experiments:

$$F = \frac{k_B T}{P} \left[\frac{1}{4} \left(1 - \frac{\Delta L}{L_c} \right)^{-2} - \frac{1}{4} + \frac{\Delta L}{L_c} \right]. \quad (1)$$

Where, ΔL is extension, T is temperature, P is persistence length, and L_c is the contour length, or the length of maximal fiber extension. The persistence length, P , determines the slope of the force versus extension curve at low strain. The contour length, L_c determines the shape of the force versus extension curve, most importantly, the onset of strain stiffening. The WLC fit in Fig. 4 shows that the Marko-Siggia WLC is a more than adequate analytical expression for modeling the single fibrin fiber mechanics. Alternative force extension models that have been applied very successfully to semiflexible biopolymer networks such as actin (34) do not fit our fibrin fiber data as well as the Marko-Siggia WLC. As we discuss in more detail below, this is because fibrin fibers do not fit the standard definition of a semiflexible polymer. Its extensibility comes from internal degrees of freedom, not from straightening of the overall contour of the fiber. A more useful model for the fiber is a network of flexible unstructured polypeptides filaments. The success of the WLC arises out of the fact that this network of molecular-sized WLCs give rise to global WLC behavior. This picture is supported by a growing consensus in the literature of fibrin mechanics that the origin of fibrin extensibility is the stretching of unstructured polypeptides (either natively unfolded or force-unfolded) within the fibrin molecule itself (10,19–21).

In the context of Eq. 1, each fiber having identical diameter corresponds to a common persistence length, P . Because P simply changes the force scale of the force versus extension properties, its value will not affect the distribution of strains within a network (though it will affect the magnitude of the force required to strain it). On the other hand, the contour length parameter, L_c , does significantly affect the stretched network configuration and strain distributions, and is the parameter that was varied to best match our experimental observations.

To give each fiber a common force versus strain relation, we modified Eq. 1 to provide force as a function of strain:

$$F = \frac{k_B T}{P} \left[\frac{1}{4} \left(1 - \frac{(\Delta L/L_0)}{(L_c/L_0)} \right)^{-2} - \frac{1}{4} + \frac{(\Delta L/L_0)}{(L_c/L_0)} \right], \quad (2)$$

$$F = \frac{k_B T}{P} \left[\frac{1}{4} \left(1 - \frac{\varepsilon}{(L_c/L_0)} \right)^{-2} - \frac{1}{4} + \frac{\varepsilon}{(L_c/L_0)} \right]. \quad (3)$$

L_c/L_0 is the adjustable parameter that determines the onset of strain stiffening. Using $(L_c/L_0) = 5$ (meaning the fibers would reach their contour lengths around strains of 4.0, although they fail before this point) provided the best correspondence to the experimental network strain distributions (Table 1). This contour length comes not from bending and straightening of the fiber itself, but from stretching out

TABLE 1 A comparison of network properties of 18 networks stretched in these experiments

	Intermediate network strain*				High network strain*			
	Max fiber strain	Change in max fiber strain (%)	Avg. fiber strain	Fiber strain SD	Max fiber strain	Change in max fiber strain (%)	Avg. fiber strain	Fiber strain SD
FXIII								
Experiment	1.09 ± 0.10	—	0.443	0.373	2.56 ± 0.18	—	1.223	0.816
WLC	1.04 ± 0.10	−4 ± 5	0.414	0.355	2.58 ± 0.09	3 ± 4	1.223	0.854
Linear	1.09 ± 0.11	1 ± 1	0.419	0.374	3.31 ± 0.17	31 ± 6	1.300	1.119
Non-FXIII								
Experiment	0.90 ± 0.08	—	0.428	0.356	1.82 ± 0.11	—	0.922	0.626
WLC	0.84 ± 0.05	2 ± 7	0.400	0.294	1.88 ± 0.09	4 ± 4	0.920	0.623
Linear	0.87 ± 0.05	1 ± 7	0.403	0.304	2.11 ± 0.14	17 ± 7	0.936	0.728

Avg. strain: average fiber strain over all of the networks; Fiber strain SD: the SD in fiber strains over all networks; Max fiber strain: average value of the most strained fiber in every network; % change in max fiber strain: on a fiber-to-fiber basis, the average percent change between the most strained fiber in the experimental network with the most strained fiber in the corresponding model network.

*Intermediate network strain is defined as the point where the AFM had moved 15 μm ; high network strain is defined as the point of network failure. Nine networks were ligated by FXIII, and nine were not. Qualitative differences were observed in the behaviors of the two types of networks, especially in the values of the most strained fibers of the network (**bold**) and the SD. Uncertainty values are listed as standard errors.

of internal molecular scale flexible segments within the subfiber structure.

Network strain distribution narrowing

A set of fibrin networks were stretched to the point of breaking and the strains of the constituent fibers were analyzed. For each experimental network, the distributions of fiber strains were compared to those from equivalent linear and WLC model network simulations. Fig. 3 compares the experimental and simulated strain data for a representative network. The experimental and WLC strain distributions differ markedly in several respects from the network of linear springs. First, the strain of the most strained fiber (Fig. 3, top trace) in the linear model is significantly higher than in the experimental data or in the WLC simulation at large AFM tip movement (Fig. 3, a–c). Second, the strain fractions of the most strained fiber in both the experimental data and WLC simulation reach a maximum and then decreases above strains of ~ 1.0 , whereas no maximum is seen in the linear model (Fig. 3, d and e). These differences were pronounced in all networks studied. The absence of decreasing strain fraction in the linear simulations indicates that this effect is due to the nonlinear force versus extension properties of the constituent fibers rather than to the generic effect of reorientation and alignment of the fibers.

Strain distributions were compared at two points: intermediate strains, where the AFM had moved 15 μm from its original location; and high strains, where the network failed (Fig. 5, inset). The intermediate strain point was chosen to fall just within the expected prestiffening linear elastic regime for all fibers. Fig. 5 shows the strain distributions for nine different networks of FXIIIa-ligated fibers at both intermediate and high strains. Although the variations in results from network to network indicate that the distribution of strains depended on the specific network geometries,

strong trends bridging all measured networks emerged from the analysis.

At intermediate strains (Fig. 5, top) the model and experimental data were statistically similar. Within uncertainties, the maximum strain (strain of most strained fiber) and the standard deviation (SD) in strain agree for the experiment, WLC, and linear model (Table 1). These results are consistent with the expectation for intermediate strain: all fibers were within the linear regime of elasticity (for experiment, WLC, and linear model networks).

On the other hand, the data and models showed distinct differences in the high strain regime (Fig. 5, bottom). The linear distribution had higher maximum strain in all cases and the lowest minimum strain for most of the networks. Comparing the most-strained fibers of each network, there was on average $31 \pm 6\%$ higher maximal strain in the linear model as compared to experiment, whereas there was only a $3 \pm 4\%$ difference between the WLC model and experiment (Table 1). As a measure of the narrowness of the strain distributions, we calculated the SD in fiber strain for each network. The average SD in the experimental data were 30% less than that of the linear network (1.1 vs. 0.82), and was still 20% lower when removing the most and least strained fiber in each network from analysis. This finding indicates the narrowing of the strain distribution occurred network wide and was not due exclusively to the behavior of the most-strained fiber. The experimental networks behaved in a manner much more consistent with the WLC model at high strains, which indicates, not surprisingly given the single fiber data (Fig. 4), that the most strained fiber in each network experienced significant strain stiffening before failure. As the network transitioned from the linear regime to the strain stiffening regime, the nonlinear elasticity of the most-strained fibers reduced the maximum fiber strain as compared to a linear network, narrowing the strain distribution and preventing strain from being concentrated into only

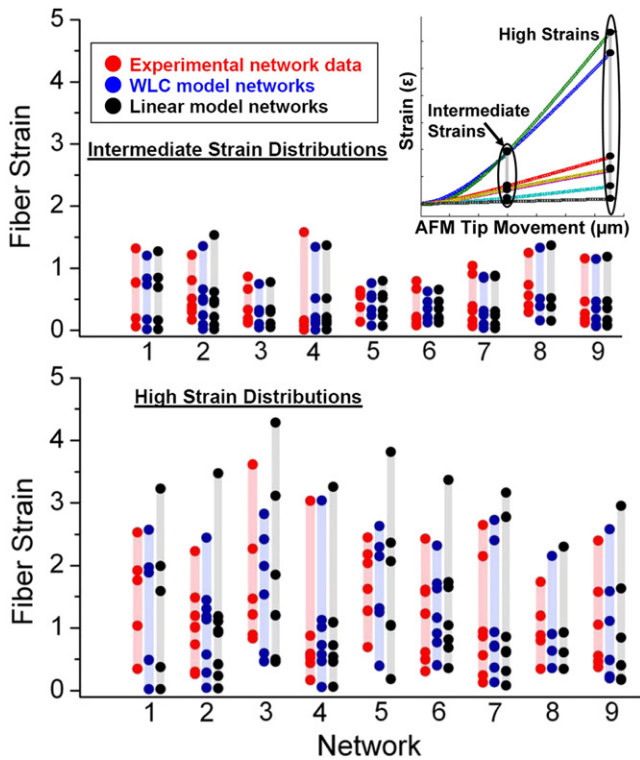


FIGURE 5 Ligated network strain distributions. A compilation of model versus experimental strain distributions for nine different network geometries formed with FXIIIa ligation. Each dot in the plots indicates the strain of a fiber within a network. The shaded bars underneath the data points are simply guides to the eye to emphasize the strain ranges. Measurements were made after $15\ \mu\text{m}$ of AFM movement (intermediate strain, *top plot*) and at the point of network failure (high strains, *lower plot*) (see *inset*). At intermediate strains there are clear variations, but no clear trends distinguish the experiment and models. At high strains, the linear model shows much higher maximum strain for all networks and lower minimum strain for all but two of the experimental networks. There is much closer correspondence between the experimental and WLC distributions (see *Table 1* for statistical analysis).

a few fibers. Although the gross features of the strain distributions showed good agreement between experiment and WLC, there are discrepancies in a fiber by fiber comparison. This discrepancy may be due largely to assumptions in the model, in particular, the use of a universal fiber diameter.

As a control, model networks composed of linear springs of varying spring constants were also tested versus the experimental results. Although the distribution of strain is altered by varying fiber stiffness within the network, the decrease in strain fraction at high strain seen in the experimental networks does not occur. Instead, the strain fraction of fibers with a linear force-extension relation approaches a constant asymptotic value regardless of stiffness. Thus, for a network of fibers of linear but variant stiffness, once the fibers align in the direction of the pull, each fiber assumes a constant share of the strain.

Physiological fibrin networks are formed in the presence of the transglutaminase FXIIIa, which incorporates covalent

bonds between monomers—a process known as cross-linking or ligation. All of the experiments and data described thus far (*Fig. 2*, *Fig. 3*, *Fig. 4*, and *Fig. 5*) reflect work on ligated fibers and networks. Studies investigating the effect of FXIIIa ligation on clot structure and mechanics show that ligated clots are stronger and more resistant to plasminogen mediated dissolution (lysis) (35) than their nonligated counterparts (6). In addition, ligation also affects the mechanics of the individual fibrin fibers in both stiffness and extensibility (18,27). As a comparison to the work with ligated networks, networks formed without FXIIIa were also stretched to gain insight into the mechanical influence of ligation. (*Fig. 6* and *Table 1*) These networks failed at significantly lower strain values than their ligated counterparts (max strain: 1.82 ± 0.11 , unligated; 2.56 ± 0.18 , ligated). However, the same trends were observed at high strains: maximum fiber strains and strain SD were lower for the experiment than in the linear models (16% and 17% lower, respectively) and in agreement with the WLC model.

DISCUSSION

We believe these studies indicate that strain stiffening of individual fibers plays a significant role in the larger scale response of fibrin networks. A closer look at the details in the plots of *Fig. 3* lends insight into the mechanisms responsible for the lower maximum strain and narrowing strain

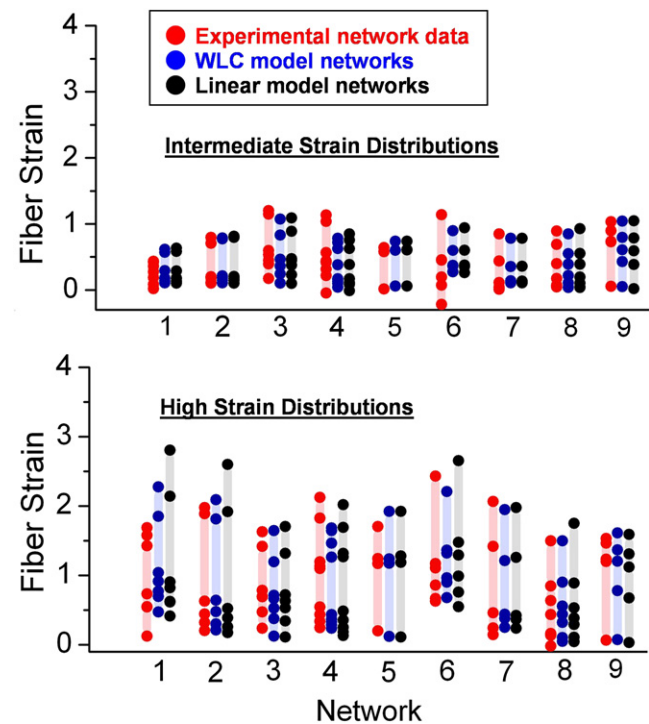


FIGURE 6 Unligated network strain distributions. A compilation of model versus experimental strain distributions for nine network geometries formed without FXIIIa cross-linking.

distribution of the fibrin networks as compared to the linear models. For the linear model, the fiber strain fraction versus AFM tip movement curves asymptotically approach a constant value at high strain (Fig. 3 *f*), indicating each fiber supports relatively constant share of the strain. For networks of strain stiffening fibers, the most strained fiber's plot trends downward indicating that the strain is shunted from areas of high strain (that have become relatively stiff) to areas of lower strain (that are relatively soft). This allows the maximum fiber strain for a given imposed network deformation to be significantly lower for the strain stiffening system than for the linear network model. The failure of the most strained fiber is a crucial event as it relates to clot strength. This initial failure will further distribute stress that may lead to severe strain concentrations and a cascading catastrophic failure of the entire network. The stiffening of the individual fibers distributes strain throughout the network, preventing the strain from being concentrated in the few lead fibers and allowing larger imposed network deformations to be accommodated by the network before fiber failure; the network is therefore effectively strengthened.

Our results underlined the importance of FXIIIa ligation on network strength (27). Fibers within ligated networks reached strains 30% higher than those in unligated networks; this result is consistent with previous measurements on single fibers (18,19). Here, however, we showed that FXIIIa ligation has a direct affect on fibrin network strength. Though biochemical factors affect many important aspects of fibrin clots (e.g., fiber diameter, cross link density, etc.), attention must be paid to how these factors affect the mechanics of the constituent fibers. Subtle biochemically induced changes in the force versus extension behavior of the individual fibers may have profound influence on overall clot mechanics.

This work also sheds light on the question of relative fiber strength versus junction strength (18). Ligated networks failed first at junctions ~30% of the time, fibers ~40% with 30% of videos inconclusive ($n = 12$). Unligated networks failed first at junctions ~45% of the time and fibers ~45% with 10% of videos inconclusive ($n = 9$). In addition, the average value for the breaking strain of the most strained fibers in the network (2.56 ± 0.18 FXIII, 1.85 ± 0.11 non-FXIII) agreed within uncertainties with published values taken from single fiber measurements of fibrin extensibility (3.32 ± 0.71 ; 2.17 ± 0.47 FXII, 2.26 ± 0.52 non-FXIII) (18,20). Although sample sizes are small, we believe this data indicates that fibrin fibers and junctions have comparable strength. More comprehensive work is needed to quantify the strength of fiber junctions and validate this small data set.

The behavior of fibrin as described within this study does not fit easily within the conventional categories of flexible, semiflexible, and stiff biopolymer networks prescribed by recent theoretical (36) and experimental reports (13,14). The fibrin fiber segments themselves behave as elastomeric

elements: extensibility of $>300\%$, strain stiffening at high strain (matching worm-like chain behavior), and elastic moduli in the MPa range (19,27,37,38). These properties do not originate from thermal fluctuations of the fiber segment's overall contour: our data (and others) show straight fibers stretching to over double their lengths before stiffening (27,39) (Fig. 1 and Fig. 2). Instead, this behavior likely has its origin in fluctuations of internal degrees of freedom residing within the fibrin molecule or subfiber structure; such high strains suggest significant alteration of the microscopic structure within the fiber. Although the persistence length of the overall fibrin fiber segment is much larger than the contour length, which would place it into the stiff filament category, the fiber is much softer (1000-fold) and more extensible (10–100-fold) in stretching than would be expected for stiff filaments with hydrogen bond mediated enthalpic elasticity (40–42). The inconsistency may be resolved by recognizing that the fiber segments themselves are behaving as networks of molecular-scale flexible filaments; that is, a network of natively unfolded or force unfolded polypeptides. This could either come from the unfolding of coiled coil domains into flexible chains as recently proposed (10), or from the stretching of an unstructured flexible region such as the α C connector (20).

This work suggests new avenues for polymeric materials design. The mechanical properties of networks might be tuned by controlling the force versus extension behavior of the constituent filaments. In the case of engineered biomaterials, this control could be gained through prescription of the primary structure of the force bearing polypeptides: the length and amino acid sequence could be tuned to adjust the onset and degree of strain stiffening and thereby select the extensibility and strength of the resultant network. For fibrin, recent single molecule and single fiber studies suggest that the unstructured α C connector region and the coiled-coil region could provide avenues for such control (20–22).

CONCLUSION

We have shown that fibrin fibers display nonlinear, strain stiffening behavior at high strains, both in the context of single fiber experiments and within a deforming network. This nonlinear behavior of individual fibers plays a crucial role in the larger scale response of fibrin networks: strain stiffening equitably distributes strain in the network. As fibers are stretched, they become stiffer than any surrounding fibers at lower strains; this allows the more strained, stiffer fibers, to distribute the strain load to the less strained fibers and reduce strain concentrations. As network strength is directly related to the failure of individual fibers with the network, this reduction of strain concentration effectively strengthens the network. This nonlinear regime of fiber elasticity is achieved before network failure and is relevant to understanding fibrin network strength. In addition, FXIIIa ligation directly affects network strength by increasing the extensibility of individual

fibers within a network. The strain concentration reduction effect may be an important mechanism in vivo, enhancing blood clot strength under the high shear conditions of the blood stream.

We thank Daniel Millard and Olamide Olusesi for help with AFM measurements and data analysis, Cory Quammen for computer programming assistance, and Lifang Ping for help with protein analysis. We also thank Oleg Gorkun, Richard Spero, and Sean Washburn for critically reviewing the document.

This work was supported by the National Institutes of Health (HL31048, P41-EB002025) and the National Science Foundation (0705977).

REFERENCES

- Weisel, J. W. 2004. The mechanical properties of fibrin for basic scientists and clinicians. *Biophys. Chem.* 112:267–276.
- Bale, M. D., and J. D. Ferry. 1988. Strain enhancement of elastic modulus in fine fibrin clots. *Thromb. Res.* 52:565–572.
- Janmey, P. A., E. J. Amis, and J. D. Ferry. 1983. Rheology of fibrin clots. VI. Stress relaxation, creep, and differential dynamic modulus of fine clots in large shearing deformations. *J. Rheol.* 27:135–153.
- Gardel, M. L., J. H. Shin, ..., D. A. Weitz. 2004. Elastic behavior of cross-linked and bundled actin networks. *Science.* 304:1301–1305.
- Janmey, P. A., U. Euteneuer, ..., M. Schliwa. 1991. Viscoelastic properties of vimentin compared with other filamentous biopolymer networks. *J. Cell Biol.* 113:155–160.
- Ryan, E. A., L. F. Mockros, ..., L. Lorand. 1999. Structural origins of fibrin clot rheology. *Biophys. J.* 77:2813–2826.
- Shah, J. V., and P. A. Janmey. 1997. Strain hardening of fibrin gels and plasma clots. *Rheologica Acta.* 36:262–268.
- Wen, Z., A. Basu, ..., P. A. Janmey. 2007. Local and global deformations in a strain-stiffening fibrin gel. *N. J. Phys.* 9:428.
- Xu, J., Y. Tseng, and D. Wirtz. 2000. Strain hardening of actin filament networks. Regulation by the dynamic cross-linking protein alpha-actinin. *J. Biol. Chem.* 275:35886–35892.
- Brown, A. E., R. I. Litvinov, ..., J. W. Weisel. 2009. Multiscale mechanics of fibrin polymer: gel stretching with protein unfolding and loss of water. *Science.* 325:741–744.
- Ferry, J. D., and P. R. Morrison. 1947. Preparation and properties of serum and plasma proteins. IX. Human fibrin in the form of an elastic film. *J. Am. Chem. Soc.* 69:400–409.
- Janmey, P. A., M. E. McCormick, ..., F. C. MacKintosh. 2007. Negative normal stress in semiflexible biopolymer gels. *Nat. Mater.* 6:48–51.
- Kang, H., Q. Wen, ..., F. C. MacKintosh. 2009. Nonlinear elasticity of stiff filament networks: strain stiffening, negative normal stress, and filament alignment in fibrin gels. *J. Phys. Chem. B.* 113:3799–3805.
- Storm, C., J. J. Pastore, ..., P. A. Janmey. 2005. Nonlinear elasticity in biological gels. *Nature.* 435:191–194.
- Heussinger, C., and E. Frey. 2006. Floppy modes and nonaffine deformations in random fiber networks. *Phys. Rev. Lett.* 97:105501.
- Onck, P. R., T. Koeman, ..., E. van der Giessen. 2005. Alternative explanation of stiffening in cross-linked semiflexible networks. *Phys. Rev. Lett.* 95:178102.
- Guthold, M., W. Liu, ..., R. Superfine. 2004. Visualization and mechanical manipulations of individual fibrin fibers suggest that fiber cross section has fractal dimension 1.3. *Biophys. J.* 87:4226–4236.
- Liu, W., L. M. Jawerth, ..., M. Guthold. 2006. Fibrin fibers have extraordinary extensibility and elasticity. *Science.* 313:634.
- Guthold, M., W. Liu, ..., S. T. Lord. 2007. A comparison of the mechanical and structural properties of fibrin fibers with other protein fibers. *Cell Biochem. Biophys.* 49:165–181.
- Falvo, M. R., D. Millard, ..., S. T. Lord. 2008. Length of tandem repeats in fibrin's α C region correlates with fiber extensibility. *J. Thromb. Haemost.* 6:1991–1993.
- Brown, A. E., R. I. Litvinov, ..., J. W. Weisel. 2007. Forced unfolding of coiled-coils in fibrinogen by single-molecule AFM. *Biophys. J.* 92:L39–L41.
- Lim, B. B., E. H. Lee, ..., K. Schulten. 2008. Molecular basis of fibrin clot elasticity. *Structure.* 16:449–459.
- Averett, L. E., C. B. Geer, ..., M. H. Schoenfish. 2008. Complexity of “A-a” knob-hole fibrin interaction revealed by atomic force spectroscopy. *Langmuir.* 24:4979–4988.
- Binnie, C. G., J. M. Hettasch, ..., S. T. Lord. 1993. Characterization of purified recombinant fibrinogen: partial phosphorylation of fibrinopeptide A. *Biochemistry.* 32:107–113.
- Gorkun, O. V., Y. I. Veklich, ..., S. T. Lord. 1997. The conversion of fibrinogen to fibrin: recombinant fibrinogen typifies plasma fibrinogen. *Blood.* 89:4407–4414.
- Doolittle, R. F. 1965. Differences in the clotting of lamprey fibrinogen by lamprey and bovine thrombins. *Biochem. J.* 94:735–741.
- Collet, J. P., H. Shuman, ..., J. W. Weisel. 2005. The elasticity of an individual fibrin fiber in a clot. *Proc. Natl. Acad. Sci. USA.* 102:9133–9137.
- Kellermayer, M. S., S. B. Smith, ..., C. Bustamante. 1997. Folding-unfolding transitions in single titin molecules characterized with laser tweezers. *Science.* 276:1112–1116.
- Oberhauser, A. F., P. E. Marszalek, ..., J. M. Fernandez. 1998. The molecular elasticity of the extracellular matrix protein tenascin. *Nature.* 393:181–185.
- Rief, M., M. Gautel, ..., H. E. Gaub. 1998. The mechanical stability of immunoglobulin and fibronectin III domains in the muscle protein titin measured by atomic force microscopy. *Biophys. J.* 75:3008–3014.
- Rief, M., J. Pascual, ..., H. E. Gaub. 1999. Single molecule force spectroscopy of spectrin repeats: low unfolding forces in helix bundles. *J. Mol. Biol.* 286:553–561.
- Schwaiger, I., C. Sattler, ..., M. Rief. 2002. The myosin coiled-coil is a truly elastic protein structure. *Nat. Mater.* 1:232–235.
- Marko, J., and E. Siggia. 1995. Stretching DNA. *Macromolecules.* 28:8759–8770.
- Palmer, J. S., and M. C. Boyce. 2008. Constitutive modeling of the stress-strain behavior of F-actin filament networks. *Acta Biomater.* 4:597–612.
- Francis, C. W., and V. J. Marder. 1988. Increased resistance to plasmic degradation of fibrin with highly crosslinked alpha-polymer chains formed at high factor XIII concentrations. *Blood.* 71:1361–1365.
- Heussinger, C., B. Schaefer, and E. Frey. 2007. Nonaffine rubber elasticity for stiff polymer networks. *Phys. Rev. E Stat. Nonlin. Soft Matter Phys E.* 76, 031906–1–031906-12.
- Aaron, B. B., and J. M. Gosline. 1981. Elastin as a random-network elastomer—a mechanical and optical analysis of single elastin fibers. *Biopolymers.* 20:1247–1260.
- Gosline, J., M. Lillie, ..., K. Savage. 2002. Elastic proteins: biological roles and mechanical properties. *Philos. Trans. R. Soc. Lond. B Biol. Sci.* 357:121–132.
- Jahnel, M., T. A. Waigh, and J. R. Lu. 2008. Thermal fluctuations of fibrin fibers at short time scales. *Soft Matter.* 4:1438–1442.
- Hearle, J. W. 2000. A critical review of the structural mechanics of wool and hair fibers. *Int. J. Biol. Macromol.* 27:123–138.
- Howard, J. 2001. *Mechanics of Motor Proteins and the Cytoskeleton.* Sinauer Associates, Sunderland, MA.
- Knowles, T. P., A. W. Fitzpatrick, ..., M. E. Welland. 2007. Role of intermolecular forces in defining material properties of protein nanofibrils. *Science.* 318:1900–1903.